Atmos. Chem. Phys., 24, 7575–7589, 2024
https://doi.org/10.5194/acp-24-7575-2024

Atmospheric Chemistry and Physics
Open Access
EGU

Measurement report: Effects of transition metal ions on the optical properties of humic-like substances (HULIS) reveal a structural preference – a case study of $PM_{2.5}$ in Beijing, China

Juanjuan Qin[1,2], Leiming Zhang[3], Yuanyuan Qin[1], Shaoxuan Shi[1], Jingnan Li[1], Zhao Shu[1], Yuwei Gao[1], Ting Qi[4], Jihua Tan[1], and Xinming Wang[2]

[1]College of Resources and Environment, University of Chinese Academy of Sciences, Beijing 100049, China
[2]Guangzhou Institute of Geochemistry, Chinese Academy of Sciences, Guangzhou 510640, China
[3]Air Quality Research Division, Science & Technology Branch, Environment and Climate Change Canada, Toronto, Canada
[4]College of Resources and Environment, University of Chinese Academy of Sciences, Beijing 100049, China

Correspondence: Jihua Tan (tanjh@ucas.ac.cn) and Xinming Wang (wangxm@gig.ac.cn)

Received: 7 November 2023 – Discussion started: 5 January 2024
Revised: 26 April 2024 – Accepted: 6 May 2024 – Published: 4 July 2024

Abstract. Humic-like substances (HULIS) are complex macromolecules in water-soluble organic compounds (WSOCs) containing multiple functional groups, and transition metal ions (TMs) are ubiquitous in atmospheric particles. In this study, potential physical and chemical interactions between HULIS and four TM species, including Cu^{2+}, Mn^{2+}, Ni^{2+}, and Zn^{2+}, were analyzed by optical method under acidic, weakly acidic, and neutral conditions. The results showed that Cu^{2+}, Mn^{2+}, and Zn^{2+} only slightly enhanced mass absorption efficiency (MAE_{365}) of HULIS in winter and had indiscernible effects on the absorption Ångström exponent (AAE) of HULIS in both seasons under all acidity conditions. All four TMs had fluorescence quenching effects on winter HULIS, and only Cu^{2+} had similar effects on summer HULIS, with the highest quenching coefficients found under weakly acidic conditions in both seasons. The ^{1}H-nuclear magnetic resonance (^{1}H-NMR) and Fourier-transform infrared (FTIR) spectra revealed that Cu^{2+} mainly bound with aromatic species and tightened the molecule structures of HULIS. The parallel factor analysis (PARAFAC) results extracted four components of HULIS, including low-oxidized humic-like substances (C1), N-containing compounds (C2), highly oxidized humic-like substances (C3), and the mixing residuals (C4), from the fluorescence spectra in both winter and summer. The spectral characteristic of HULIS with Cu^{2+} additions under three acidity conditions indicated that electron-donating groups of HULIS mainly corresponded to C1 and C3, with Cu^{2+} binding with HULIS by replacing protons, while electron-withdrawing groups of HULIS could correspond to C2, with its connection with Cu^{2+} through electrostatic adsorption or colliding-induced energy transfer.

1 Introduction

Atmospheric particles, consisting of both organic and inorganic substances, have significant impacts on the natural environment, climate, and human health. Humic-like substances (HULIS) and transition metal ions (TMs) are among the major organic and inorganic fractions and can substantially affect the physical and chemical properties of atmospheric particles (Hawkins et al., 2016; Zanca et al., 2017; Frka et al., 2018; Ma et al., 2019). HULIS and many TMs, such as Fe, Cu, Mn, V, Cr, and Co, have negative impacts on human health since they can promote the generation of reactive oxygen species (ROS), which cause an inflammatory response of the human respiratory system (Verma et al.,

2012; Gali et al., 2015; Lin and Yu, 2019; Zhang et al., 2022). HULIS are known as a mixture of macromolecular organic compounds, containing aromatics and aliphatic species with multiple oxygenated functional groups like carbonyls, hydroxyl, nitrate, and nitroxy-organosulfate (Win et al., 2018; Huang et al., 2022; Zhang et al., 2022). TMs can transfer electrons and participate in chemical reactions or serve as a catalyst, especially in atmospheric photochemistry (Mao et al., 2013; Guasco et al., 2014).

Considering that HULIS and TMs are both active chemical components of atmospheric particles, the significance of their co-effects is apparently conceivable. Early studies have demonstrated that HULIS can enhance the solubility of TMs by organic complexation (Paris and Desboeufs, 2013; Scheinhardt et al., 2013) and TMs might mediate organic transformation processes and induce the formation of light-absorbing secondary water-soluble organics and water-insoluble abiotic polymers (Slikboer et al., 2015). More recent studies focused on the oxidation potentials and ROS formation or other metal-induced photochemical reactions of TMs (Fe^{2+}, Cu^{2+}, and Mn^{2+}) in combination with HULIS (Gonzalez et al., 2017; Lin and Yu, 2019; Ye et al., 2021). The mixture of TMs and HULIS could exhibit synergistic or antagonistic effects on ROS formation associated with the chemical composition of HULIS. Moreover, TMs can also bind with HULIS and directly affect the light-absorption properties of HULIS (Fan et al., 2021; Wang et al., 2021).

To reveal the linkage between HULIS and TMs in atmospheric chemistry, this study characterized the varying optical and chemical properties of HULIS with the addition of different TM species under three different levels of acidity. The effects of TMs on light absorption of HULIS and the TM-sensitive fraction of HULIS were determined by optical spectra, and parallel factor analyses (PARAFACs) were performed to unveil the susceptive fluorescent components. The interaction between Cu^{2+} and HULIS was further analyzed for its prominent effects, and the potential reaction mechanisms were deduced based on the structural and optical variation scenarios. Results from the present study advanced our understanding on the physical and chemical characteristics and transformations of HULIS, and especially the physical and chemical connections between HULIS and TMs.

2 Methods

2.1 Sample extraction and titration

In the present research, two concentrated HULIS solutions were extracted from daily $PM_{2.5}$ samples collected in summer and winter of 2016 (30 samples in each season) in Beijing, and the detailed sample information can be found elsewhere (Qin et al., 2022). The HULIS isolation was mainly based on the method established by Lin et al. (2010), with some procedures adjusted for practical reasons. Firstly, water-soluble organic compounds (WSOCs) were ultrasonically extracted from 30 or 60 daily $PM_{2.5}$ filter samples ($D = 2$ cm; 30 pieces for winter and 60 pieces for summer) using 200 mL Milli-Q water three times and filtered using 0.22 µm membranes. The liquids were then separated by solid phase extraction (SPE) cartridges (Oasis HLB; 6cc, 500 mg per cartridge; Waters, USA), rinsed with 10 mL water, and pumped to dry. The cartridges were eluted with 10 mL methanol afterwards. Finally, the eluants were evaporated to dryness by N_2 at room temperature and redissolved into 200 mL ultrapure water to obtain a HULIS stock solution.

Before metal ion titration, the HULIS stock solutions were diluted 10-fold, and the total organic carbon (TOC) concentration was determined by a TOC analyzer (Multi N/C 3100; Germany), with the carbon concentrations of 1.9 mg L^{-1} for winter HULIS and 1.6 mg L^{-1} for summer HULIS. The original acidity of HULIS was determined by a pH meter (Mettler Toledo, Switzerland) before and after dilution. In both winter and summer, triplicate 600 mL of diluted HULIS solutions was separately added to 1 L sealed vials to obtain weakly acidic HULIS (pH = 5.65 for winter and pH = 5.92 for summer), acidic HULIS (pH ≈ 3.0; by 0.05 M H_2SO_4), and neutral HULIS (pH ≈ 7.5; by 0.1 M NaOH), respectively. Considering the instability of the natural pH gradient, excessive base solution was added to ensure the solution pH was around neutral before measurement.

Four transition metal ions that are relatively rich in $PM_{2.5}$ in Beijing and can form a complex with HULIS were considered, including Cu^{2+}, Zn^{2+}, Mn^{2+}, and Ni^{2+} (Wang et al., 2021). Titration experiments were conducted by adding 0–526.32 µL corresponding metal sulfate solutions (0.01 M) and 9 mL diluted HULIS solution to a 10 mL amber volumetric flask, and ultrapure water was then added to obtain samples containing TM concentrations of 0, 20, 50, 100, 200, 300, and 500 µM. The titrated solutions were shaken for 12 h at room temperature to ensure complexation equilibrium, and the pH of all titrated samples was detected again before spectral analysis.

2.2 Spectral analysis

The optical properties of HULIS with the addition of TMs (0–500 µM) were analyzed by UV–Vis and fluorescence spectrophotometers under acidic, neutral, and neutral pH. The chemical properties of HULIS before and after adding TMs were analyzed by ^{1}H-nuclear magnetic resonance (^{1}H-NMR) and Fourier-transform infrared (FTIR).

The UV–Vis absorption spectra of WSOCs and HULIS were measured by a UV–Vis photometer (Agilent Technologies), covering a wavelength range of 200–500 nm, with an interval of 1 nm, using a scanning speed of 200 nm min^{-1}. The three-dimensional fluorescence spectra were measured by an Agilent Technologies photometer under the following conditions: excitation wavelength (Ex) of 200–400 nm, with a step length of 5 nm and slit width of 10 nm; emission

wavelength (Em) of 250–500 nm, with a step length of 5 nm and slit width of 5 nm; scanning speed of 2400 nm min^{-1}; and automatic response time. The sample pool for UV–Vis and three-dimensional fluorescence uses a quartz colorimeter with a light path of 1 cm. The limit of detection for UV–Vis and fluorescence analysis was estimated to be 2 times their respective standard deviation of blanks, which were 0.005 and 0.01 absorption unit, respectively.

The infrared spectra of HULIS for wavenumbers between 4000 and 400 cm^{-1} were measured by an FTIR spectrometer (Thermal Fisher; Nicolet IS10) at room temperature. The essential extraction of HULIS for FTIR measurements was the same as those described in Sect. 2.1 above, except that around 1 mg of the HULIS (dried by a gentle stream of N_2 at room temperature, 25 °C) was directly mixed with 60 mg KBr and dried in a drying oven rather than redissolved by water. The mixtures were then ground and pressed into firm tablets for analysis. A 600 MHz NMR spectrometer (Bruker; AVANCE III 600 M) was applied for ^{1}H-NMR spectra measurements. Dried HULIS samples of about 5 mg were redissolved in 1 mL D_2O for ^{1}H-NMR detection.

2.3 Data analysis

2.3.1 Mass absorption efficiency and absorption Ångström exponent

The mass absorption efficiency (MAE; 10^3 AU cm^2 mg^{-1}) of HULIS and the absorption Ångström exponent (AAE) were obtained as follows (Kirillova et al., 2014; Saleh et al., 2014):

$$\mathrm{MAE} = (A_\lambda - A_{700}) \times \frac{\ln(10)}{C_{\mathrm{spcies}} \times L}, \quad (1)$$

$$A_\lambda = K\lambda^{-\mathrm{AAE}}, \quad (2)$$

where A_λ is light absorbance at wavelength λ, C_{species} is the chemical concentration of organic compounds (WSOCs and HULIS in the present research), L is the light path length (1 cm), K is a scaling constant, and the fitting wavelength of AAE is 300–400 nm.

2.3.2 Fluorescence indices

Fluorescence indices based on intensity ratios may provide clues about the condensation state of WSOCs. The average fluorescence intensity (AFI) is the mean intensity of an excitation–emission matrix (EEM) spectrum; the specific fluorescence intensity (SFI) is the fluorescence intensity per unit of TOC (mg L^{-1}) (Kalbitz et al., 2000). The biological index (BIX) reflects the freshness of microbially produced DOM (Parlanti et al., 2000), with a high BIX value (> 1) corresponding to a predominantly microbial-derived organic matter and a value of < 0.6 indicating fewer microbial-originated DOM (Qin et al., 2018). BIX is calculated as follows:

$$\mathrm{BIX} = \frac{\mathrm{EEM}_{\mathrm{Ex}_{200-310},\mathrm{Em}_{250-380}}}{\mathrm{EEM}_{(\max(\mathrm{Ex}_{200-310},\mathrm{Em}_{420-435}))}}. \quad (3)$$

The fluorescence lifetime for HULIS was estimated by a formula derived from the Strickler–Berg equation (Strickler and Berg, 1962). The τ_0/ρ ratio comprehensively reflects the fluorescence intrinsic lifetime (related to the fluorophore type) and fluorophore density (associated with the molecular structure); a large τ_0/ρ can result from a long fluorescence lifetime or a small fluorophore (Xiao et al., 2018).

$$\tau_0/\rho = c2.88 \times 10^{-12} n^2 \frac{\int_{\mathrm{Em}} \mathrm{FI}(\nu)\mathrm{d}\nu}{\int_{\mathrm{Em}} \nu^{-3}\mathrm{FI}(\nu)\mathrm{d}\nu} \int_{\mathrm{Ex}} \mathrm{UVA}(\nu)\mathrm{d}\nu^{-1} \quad (4)$$

where τ_0 is the intrinsic lifetime (ns), ρ is the density of fluorophore in the organics (mmol fluorophore per g C), c is the total organic concentration (mg C L^{-1}), n is the refractive index of the solution ($n^2 \approx 1.8$), ν is the excitation or emission wavenumber (cm^{-1}), UV is the UV–Vis absorbance (absorption unit, AU), and FI is the fluorescence intensity (Raman unit, RU).

The Stokes shift (SS) can reflect the fluorescence energy of organics (Xiao et al., 2020; Yu et al., 2020) and is defined as $\mathrm{Ex}^{-1} - \mathrm{Em}^{-1}$ nm^{-1}, demonstrating the energy loss of the excited fluorophore due to internal conversion during relaxation (Lakowicz, 2006). AvgSS were defined as the intensity-weighted average Stokes shifts in HULIS (Xiao et al., 2019).

2.3.3 Parallel factor analysis (PARAFAC)

PARAFAC model can decompose complex EEM spectra into several main components by a statistical method. The excitation spectrum, emission spectrum, and scores of each component are as follows:

$$x_{ijk} = \sum_{f=1}^{F} a_{if} b_{jf} c_{kf} + \varepsilon_{ijk}, \quad i = 1, \ldots, I, j = 1, \ldots, J, k = 1, \ldots, K, \quad (5)$$

where x represents the fluorescence intensity, f is the number of components resolved by PARAFAC, a is proportional to the concentration of the fth component, and b and c are the scaled estimates of the emission and excitation spectra. The subscript i is the sample number and j and k represent emission and excitation wavelength, respectively. Before performing PARAFAC, all EEM data were normalized to the unit norm to reduce concentration-related collinearity and avoid extremely different leverages (Wang et al., 2020). Tucker's congruence coefficient (TCC) was determined for each excitation spectrum and emission spectrum, and a threshold of 0.95 was applied to confirm the spectral congruence. The model was determined by half-split validation.

3 Results and discussion

The light absorption and fluorescence efficiencies of winter and summer HULIS in acidic, weakly acidic, and neutral environments are depicted in Fig. 1, and the spectra-derived indices are listed in Table 1. Generally, the overall

light absorption efficiencies (represented by MAE) of winter HULIS were higher than those in summer, and the AAE showed a reverse trend, indicating higher light absorption abilities of winter than summer samples (Mo et al., 2021). The MAE and AAE of HULIS on three acidity levels in both seasons were consistent with those reported in our previous research, with the average MAE_{365} at 0.011 ± 0.00 in winter and 0.005 ± 0.001 in summer and the corresponding average $AAE_{300–400\,nm}$ at 6.46 ± 0.86 and 6.97 ± 0.83, respectively (Qin et al., 2022), which were comparable with those of Gosan, South Korea (Kirillova et al., 2014), Hong Kong SAR, China (Ma et al., 2019), and Tibet, China (Wu et al., 2019), but lower than those of biomass burning sources (Park et al., 2016).

The fluorescence efficiencies of winter HULIS (represented by SFI and AFI per TOC) were higher than those of summer HULIS as well (Fig. 1), and the fluorescence indices reveled some structural differences. The SFI spectra of HULIS mainly exhibited two fluorescence peaks at wavelengths of Ex = 225–230 nm and Em = 380–400 nm and Ex = 325–330 nm and Em = 395–400 nm in both seasons, with the peaks being roughly characterized as fulvic-acid-like groups and protein-like groups, respectively. The Stokes shift index of AvgSS could be associated with the hydrophobicity or hydrophilicity of organics, with a low AvgSS implying a relatively high hydrophilicity and a high one implying a high hydrophilicity (aromaticity or humification degree) (Xiao et al., 2019). Thus, the higher AvgSS of winter HULIS indicated a higher hydrophilicity compared to that in summer.

The different optical properties of HULIS between winter and summer mainly resulted from divergent chemical structures. Our previous research had revealed that winter HULIS contained more unsaturated structures and were relatively hydrophobic, leading to the higher light absorption and fluorescence efficiencies, while summer HULIS were rich in oxidized species and functional groups and were more hydrophilic (Qin et al., 2022). Baduel et al. (2011) evaluated the varying optical properties of HULIS during O_3 oxidation and found the C=O and COOH groups of HULIS increased with oxidation. However, Yang et al. (2021) found that O_3 oxidation of humic acid could consume some functional groups like aromatic C=C, OH, C=O, COOH, and COO^-, causing a decrease in MAE and an increase in AAE, and these divergences were ascribed to the different structures of HULIS. The different structures of HULIS between winter and summer could lead to not only the varied optical properties, but also the distinctive behaviors of HULIS with other species coexisting in the atmospheric environment. Therefore, it is necessary to analyze the relations between TMs and HULIS for winter and summer HULIS separately.

3.1 Effects of TMs on the light absorption properties of HULIS

The gradients of MAE_{365_i}/MAE_{365_0} and $AAE_{300–400\,nm}$ for HULIS with TM (Cu^{2+}, Mn^{2+}, Ni^{2+}, and Zn^{2+}) concentrations ranging from 0 to 500 µM under three acidity conditions are depicted in Fig. 2 and the whole MAE spectra are exhibited in Figs. S1 and S2 in the Supplement. For winter HULIS, in the acidic environment, the addition of Mn^{2+}, Ni^{2+}, and Zn^{2+} at low concentrations (< 50 µM) could induce a decrease of 14 %–16 % in MAE_{365}; further increasing TM concentrations had little effect on MAE_{365}, whereas Cu^{2+} showed minimal effects on MAE_{365}, which only decreased MAE_{365} by 5 % with increasing TM concentrations. These results were consistent with a previous study which found that the light absorption capacity of the atmospheric HULIS solution in the Cu^{2+}-, Al^{3+}-, or Zn^{2+}-coupled system can be enhanced to 5 %–35 % (a mean of 19 %) (Li et al., 2022). Under weakly acidic environment, a small amount of any TMs (0–50 µM) could induce an evident increase of MAE_{365} at a range of 16 % to 20 %. MAE_{365} then became steady or slightly decreased with further increasing TM concentrations. As for the neutral environment, the addition of Cu^{2+} could lead to up to a 9 % increase in MAE_{365}, but Cu^{2+} showed inhibiting effects on MAE_{365} in cases with additions of Mn^{2+}, Ni^{2+}, or Zn^{2+}, with the maximum decrease of 11 %, 7 %, and 14 %, respectively. Nevertheless, TMs could only change the $AAE_{300–400\,nm}$ of HULIS slightly, and the solution acidity sieved the initial $AAE_{300–400\,nm}$ of HULIS; besides, the TM concentrations had inconspicuous effects on the regularity. An exception was observed for Ni^{2+} because of its self-absorption between 350 and 400 nm, leading to the continuously reduction of $AAE_{300–400\,nm}$ with increasing $[Ni^{2+}]$.

For summer HULIS, Cu^{2+}, Mn^{2+}, and Zn^{2+} could cause fluctuations in MAE_{365} with increasing metal ion concentrations under acidic and neutral environments, and they also inhibited the light absorption efficiencies of HULIS under weakly acidic environment. Likewise, Ni^{2+} could enhance the MAE_{365} of HULIS under all acidity conditions because of the increase in absorption generated by increasing Ni^{2+} concentrations. The $AAE_{300–400\,nm}$ of HULIS had a subtle variation when adding Cu^{2+}, Mn^{2+}, and Zn^{2+} in acidic and neutral environments, indicating that the TM–HULIS mixtures might not compose complexations or their complexes exhibited no structural difference. Yet when the solution was weakly acidic, the $AAE_{300–400\,nm}$ exhibited sharp fluctuations with increasing Mn^{2+} and Zn^{2+} and even increased with increasing Cu^{2+} concentrations.

Table 1. The light absorption and fluorescence indices of HULIS under three acidity conditions.

	Winter				Summer			
	Acidic	Weakly acidic	Neutral	Mean ± SD	Acidic	Weakly acidic	Neutral	Mean ± SD
MAE_{365}^{a}	0.011	0.011	0.011	0.011 ± 0.00	0.006	0.004	0.006	0.005 ± 0.001
$AAE_{300–400\,nm}$	7.05	6.86	5.47	6.46 ± 0.86	6.97	7.80	6.15	6.97 ± 0.83
AFI/TOC[b]	0.79	0.62	0.58	0.66 ± 0.11	0.10	0.10	0.09	0.10 ± 0.01
BIX	1.07	0.96	0.99	1.00 ± 0.05	0.98	0.90	0.90	0.93 ± 0.05
AvgSS	1.54	1.54	1.54	1.54 ± 0.00	1.01	0.90	0.91	0.94 ± 0.06
τ_0/ρ	0.15	0.24	0.13	0.17 ± 0.06	0.56	0.92	0.60	0.69 ± 0.19

[a] 10^3 AU cm^2 mg C^{-1}. [b] RU L mg C^{-1}.

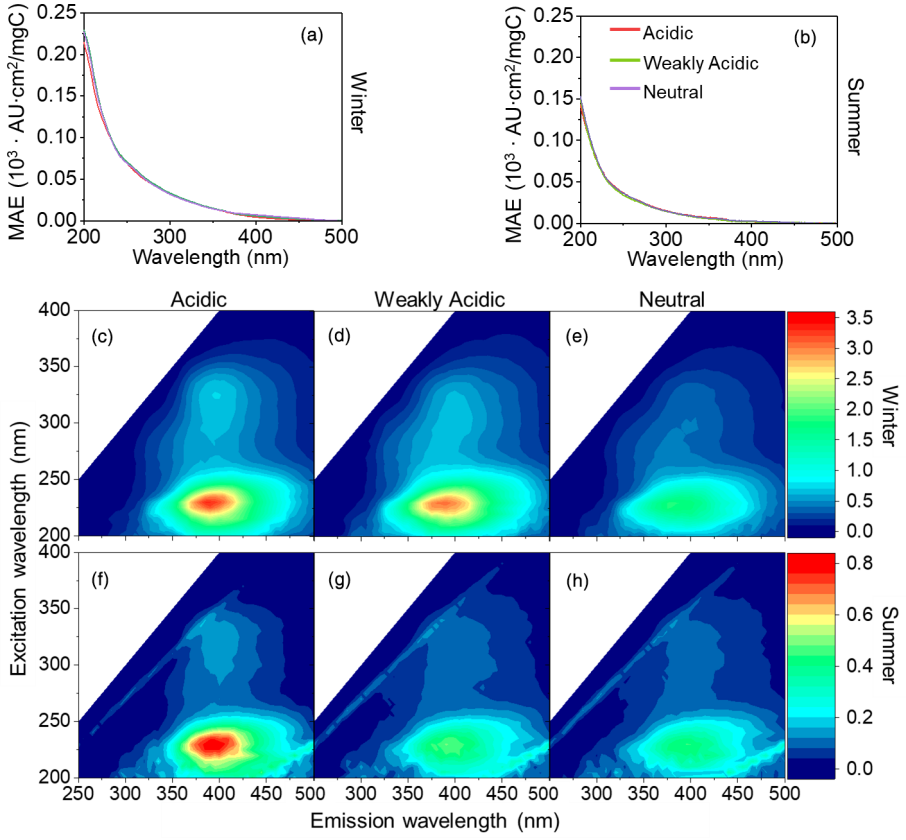

Figure 1. The MAE **(a–b)** and SFI **(c–h)** spectra of winter and summer HULIS under three acidity conditions.

3.2 Effects of TMs on the fluorescence properties of HULIS

The effects of TMs on the fluorescence indices of HULIS in different acidity environments are shown in Figs. 3 and 4 and the fluorescence spectral variations are provided in Figs. S3 and S4. Obviously, all four TMs showed quenching effects on the AFI of HULIS with fiddling seasonal or acidity-dependent differences, with the effectiveness ranking on the order of $Cu^{2+} > Mn^{2+} \sim Ni^{2+} > Zn^{2+}$. At the maximum TM concentration of 500 µM, AFI of winter HULIS reduced by 5 %–21 %, 5 %–11 %, and 7 %–28 % and of summer HULIS reduced by 8 %–22 %, 12 %–39 %, and 5 %–26 % under acidic, weakly acidic, and neutral environments, respectively.

The effects of TMs on fluorescent HULIS could be evaluated by the Stern–Volmer equation. Supposing metal ions only singly bonded with HULIS molecules, the values of the quenching constant (k) obtained from relations between TM concentrations and total fluorescence intensities of HULIS are listed in Table 2. Briefly, for winter HULIS, all TM

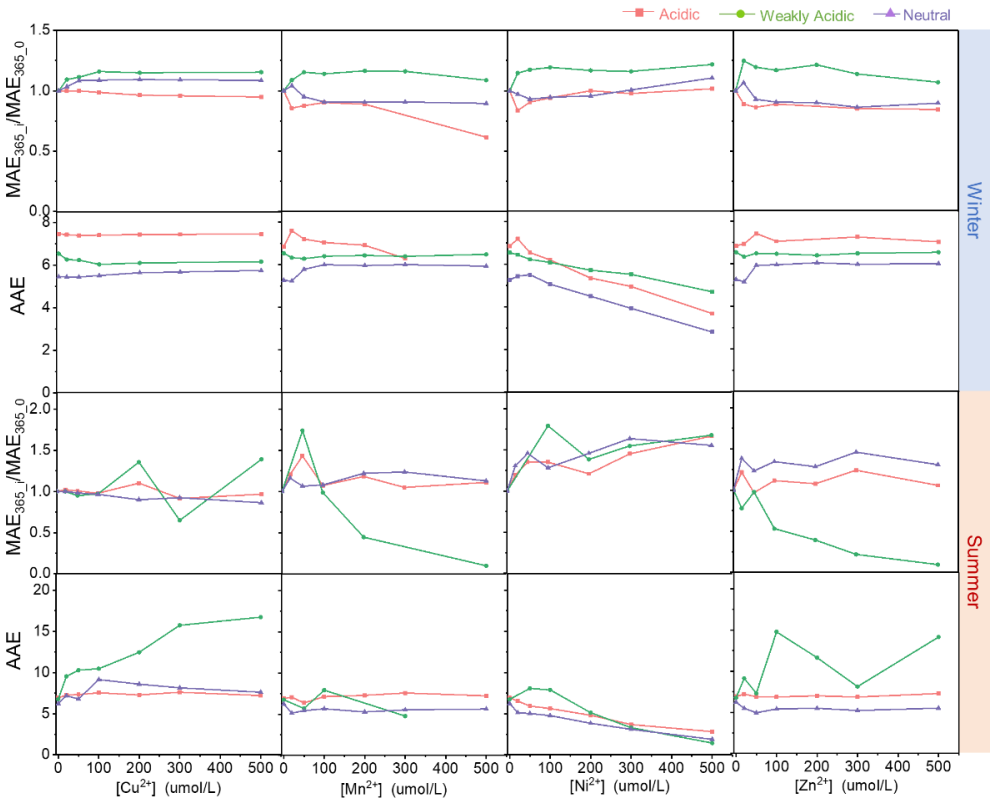

Figure 2. The light absorption indices of HULIS with additions of TMs under different acidity conditions.

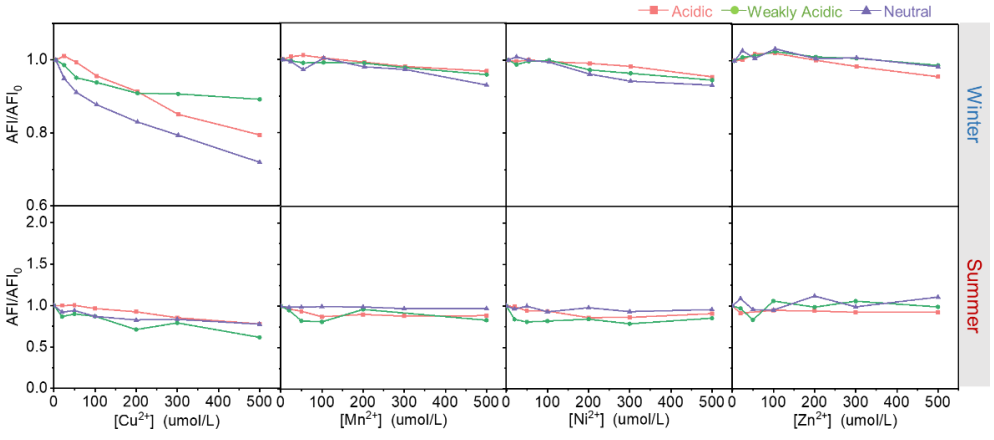

Figure 3. The average fluorescence intensities of HULIS with additions of Cu^{2+}, Zn^{2+}, Mn^{2+}, and Ni^{2+} under different acidity conditions in winter and summer.

species had significant linear correlations with AFI/AFI_0 ($R^2 > 0.6$). Cu^{2+} and Mn^{2+} had the largest k constants in acidic and neutral environments and a relatively low k in the weakly acidic environment, indicating that Cu^{2+} and Mn^{2+} might mainly bond with organic groups that dissociated in acidic or neutral environments. Ni^{2+} had the same k in weakly acidic and acidic environments and a larger k in the neutral environment, indicating that Ni^{2+} might prefer to bond with neutral HULIS. Similarly, Zn^{2+} had a larger k in the acidic environment, indicating a preference for the acidic environment for the complexation of Zn^{2+} and HULIS. For summer HULIS, Cu^{2+} still had a significant and large k in acidic and neutral environments and a relatively low k in the neutral environment. Mn^{2+} only had a relatively large k in the acidic environment and a low k in the neutral environment but no statistically significant k in weakly acidic environment. Besides, AFI/AFI_0 of HULIS with Ni^{2+} and

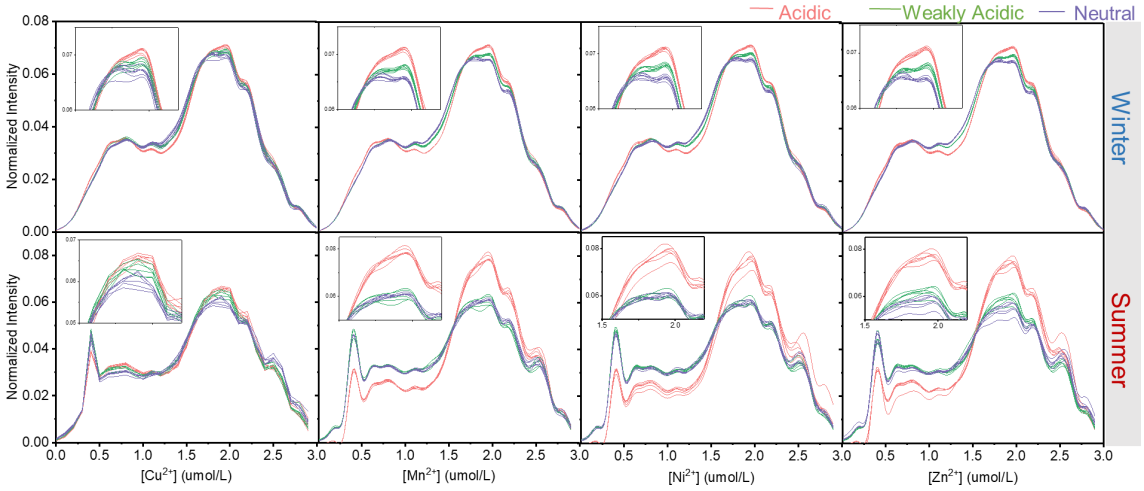

Figure 4. The Stokes shift spectra of HULIS with additions of Cu^{2+}, Zn^{2+}, Mn^{2+}, and Ni^{2+} under different acidity conditions.

Zn^{2+} also had a non-significant k, indicating negligible interactions between fluorescent HULIS and these two ions.

Although TMs showed quenching effects on HULIS, the locations of fluorescence peaks rarely moved with increasing TM concentrations. Thus, the fluorescence-spectra-based indices only show minimal variations under different acidity conditions with increasing metal ions concentrations. In Fig. 4, the Stokes shift spectra of HULIS separated into groups under three acidity conditions for both seasons. Only the addition of Cu^{2+} could hierarchically distribute the spectra slightly. The other three TMs showed inconspicuous effects, indicating that they could not cause substantial structural variations in fluorescent HULIS, as can be better presented visually by the ratio of $AvgSS_0$ to $AvgSS_i$ (Fig. 5). Additionally, the addition of Mn^{2+}, Ni^{2+}, and Zn^{2+} did not change the τ_0/ρ of HULIS either, which might confirm that they did not bind with HULIS molecules since fluorescent lifetime is a sensitive indicator vulnerable to the micro-environment surrounding detected objects (Coble et al., 2014).

3.3 Distinguishing the varying fractions of HULIS with the addition of TMs

To further identify the response of specific HULIS compounds to TMs, PARAFAC methods were applied to distinguish the varying groups of HULIS with the addition of different TM species. In general, four compounds (C1–C4) were sorted out from EEM spectra of winter and summer HULIS, and they were characterized as low-oxidized humic-like substances (C1), N-containing compounds (C2), highly oxidized humic-like substances (C3), and mixing residuals (C4), respectively (Chen et al., 2016). The constitution of C1–C4 in winter and summer HULIS under different acidity levels is listed in Table 3.

Forming the correlations between the F / F_0 ratio and TM concentrations of fluorophores, C1–C4, shown in Figs. 6 and 7 (corresponding Stern–Volmer results listed in Tables S1 and S2 in the Supplement), it was obvious that the intensities of the four fluorophores had increasing or decreasing tendencies in response to the acidity and TM species because of the divergent acid or base groups of HULIS. In the case of winter HULIS under acidic environment, Cu^{2+} could induce a substantial fluorescence-quenching effects on C1 and C4 and a concurrent modest fluorescence-increasing effects on C3, Mn^{2+} and Ni^{2+} exhibited weak fluorescence-quenching effects on C1 and C3, and Zn^{2+} exhibited weak fluorescence-quenching effects on C1 and C4. In the weakly acidic environment, all of the four TMs exhibited discernible quenching effects on C2 and C3, with Cu^{2+} manifesting as the most potent quencher. In the neutral environment, Cu^{2+} significantly quenched the fluorescence intensities of C1, C2, and C4; Ni^{2+} displayed modest quenching effects only on C3; and other metal ions showed inconspicuous fluorescence-quenching or fluorescence-enhancing effects.

As for summer HULIS, only Cu^{2+} exhibited notable quenching effects on fluorophores, C1–C4, while Mn^{2+}, Ni^{2+}, and Zn^{2+} showed rather minimal or erratic effects under all acidity conditions. In acidic and weakly acidic environments, Cu^{2+} could reduce the fluorescence intensity of C1–C3, and contributions of C4 to total fluorescence intensities gradually increased. For the neutral environment, Cu^{2+} exhibited pronounced fluorescence-quenching effects on C2 and mild reduction tendencies for C1 and C3. Because of the minimal quenching effects of Mn^{2+}, Ni^{2+}, and Zn^{2+} on C1–C4, most of the correlation coefficients (R^2) between F / F_0 and metal ion concentrations were small, indicating the insignificant effects of Mn^{2+}, Ni^{2+}, and Zn^{2+} on HULIS.

In light of the above analysis, it was obvious that Cu^{2+} demonstrated much more significant effects on optical properties of HULIS than the other three metal ions, which might

Table 2. The fluorescence quenching coefficients of TMs and HULIS obtained from Stern–Volmer equation.

		Cu^{2+}		Mn^{2+}		Ni^{2+}		Zn^{2+}	
Stern–Volmer	Acidity	$k \times 10^3$	R^2	$k \times 10^3$	R^2	$k \times 10^3$	R^2	$k \times 10^3$	R^2
Winter	Acidic	0.60	0.99	0.10	0.98	0.10	0.95	0.20	0.98
	Weakly acidic	0.10	0.86	0.08	0.91	0.10	0.95	0.07	0.83
	Neutral	0.60	1.00	0.10	0.68	0.20	0.90	0.07	0.58
Summer	Acidic	0.60	0.99	0.20	0.38	−0.02	0.79	0.01	0.02
	Weakly acidic	1.00	0.82	−0.10	0.02	−0.04	0.05	−0.20	0.13
	Neutral	0.40	0.88	0.05	0.63	0.05	0.08	−0.20	0.16

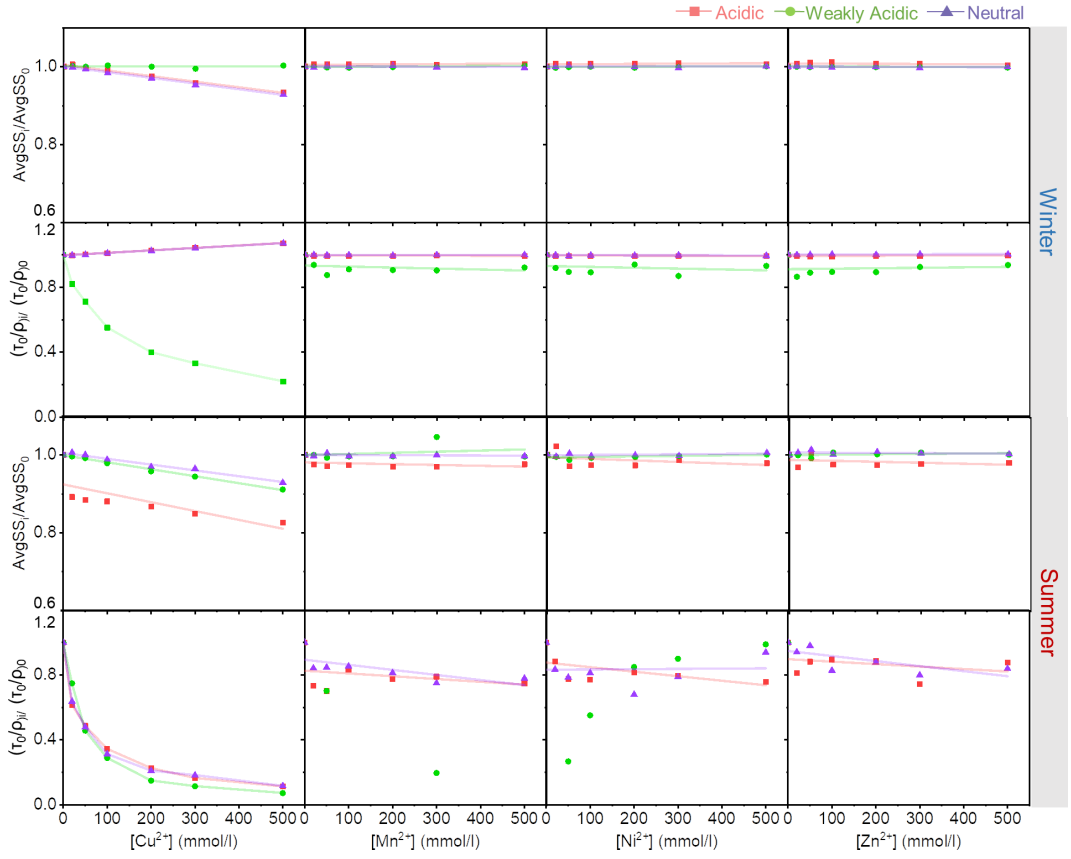

Figure 5. The fluorescence indices of HULIS with increasing Cu^{2+}, Zn^{2+}, Mn^{2+}, and Ni^{2+} concentrations under different acidity conditions.

be because of their disparate complexing abilities (Fan et al., 2021). Li et al. (2022) found that with increasing Fe^{3+}, Al^{3+}, and Cu^{2+} concentrations, the fluorescence intensities of highly oxidized HULIS decreased and those of low-oxidized HULIS gradually increased, and they ascribed these phenomena to the fluorophore blue shifts in highly oxidized HULIS induced by complexation. Likewise, some other studies observed strong bonds between Cu^{2+} and atmospheric organic matter (Wang et al., 2021; Ma et al., 2022). However, the detailed mechanisms causing the different complexation results of TMs remained unclear.

It was noticed that studies on the effects of TMs on optical properties of fulvic acid and humic acid had been conducted in earlier years in surface water rather than an atmospheric environment, which provided inspiration for the present study. For example, it was reported in the 1980s that Cu^{2+} posed greater fluorescence-quenching effects on fulvic acid than Co^{2+} and Mn^{2+}, and it was thus proposed that Cu^{2+} bound internally to fulvic acid, while Co^{2+} and Mn^{2+} might be only externally attached to organics via electrostatic attraction (Ryan et al., 1983). Other studies found that Cu^{2+} had stronger complexation capabilities compared

Table 3. The PARAFAC decomposed fractions of HULIS for winter and summer under three acidity conditions.

		C1	C2	C3	C4	Total fluorescence intensity
Winter	Acidic	42 %	19 %	24 %	15 %	805.52
	Weakly acidic	29 %	24 %	27 %	19 %	869.69
	Neutral	22 %	27 %	29 %	22 %	587.49
Summer	Acidic	50 %	28 %	20 %	2 %	192.09
	Weakly acidic	23 %	26 %	18 %	32 %	179.17
	Neutral	16 %	32 %	16 %	36 %	161.00

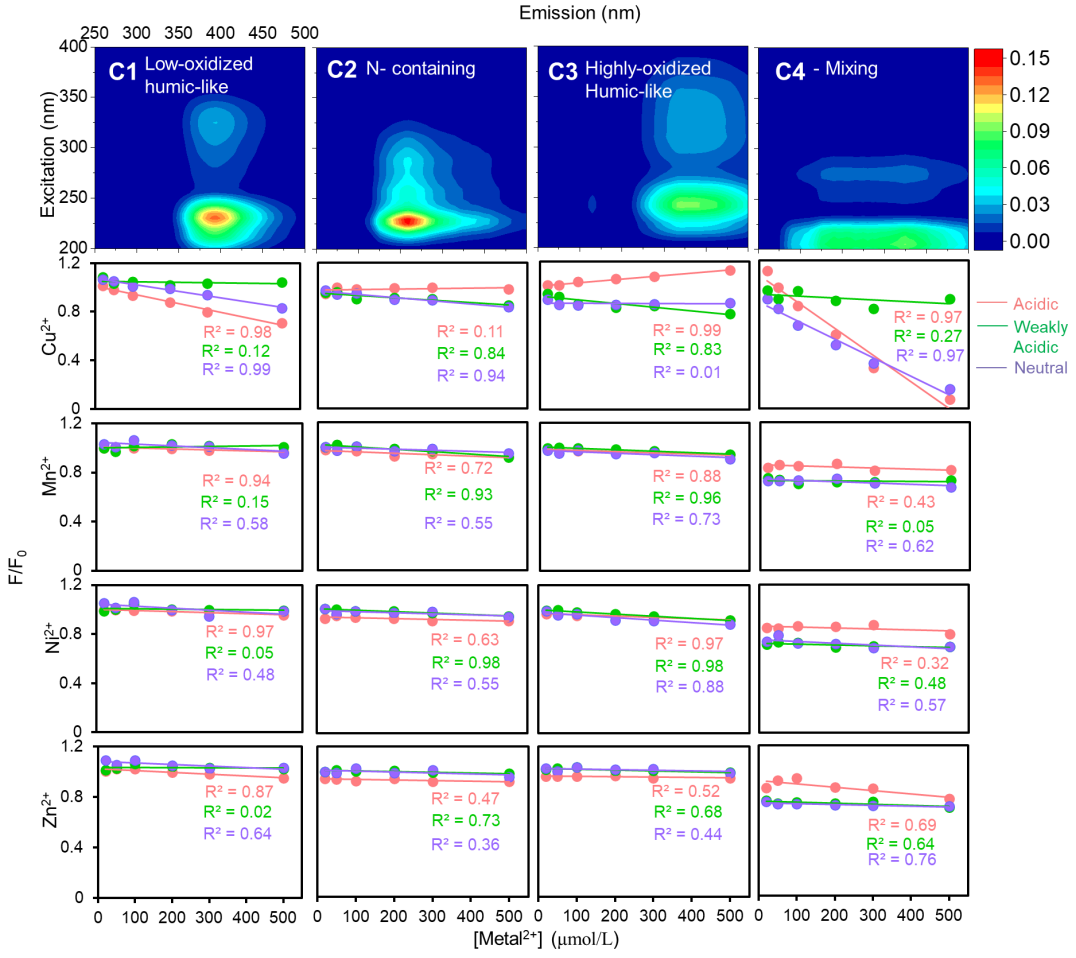

Figure 6. The changing patterns of four fluorophores with TMs under different acidity conditions for winter HULIS.

to the other divalent transition metal ions, such as Pb^{2+}, Cd^{2+}, Ni^{2+}, and Zn^{2+} (Yamashita and Jaffe, 2008; Chen et al., 2015; Huang et al., 2018). With the application of two-dimensional infrared correlation spectroscopy and synchronous and asynchronous fluorescence spectroscopy analysis, carboxyl and polysaccharide groups were found to bind fast with Cu^{2+}; and the bonding of Cu^{2+} with phenolic and aromatic carboxyl groups altered the molecule vibration of organics, inducing fluorescence quenching. Besides, Cu^{2+} could bind with several amide and aliphatic groups (protein-like), leading to fluorescence quenching. More recently, Zhu et al. (2021) suggested that the small atomic radius and paramagnetic properties might result in the unique response of Cu^{2+} to carboxyl groups, and thus a strong complexation ability with DOM. Considering the smaller molecules and aromatic structures of HULIS compared to humic substances in water, Cu^{2+} continued its specialty of significant fluorescence quenching effects on HULIS, whereas bonds between

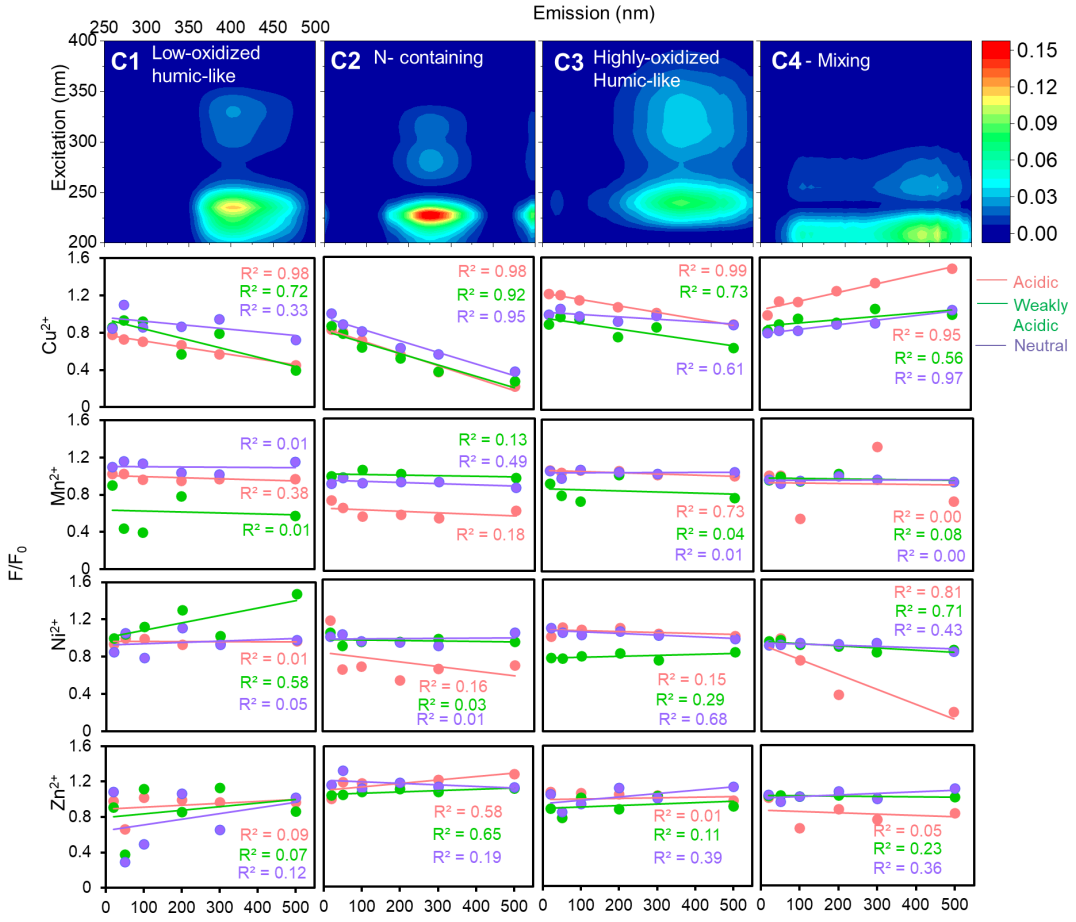

Figure 7. The changing patterns of four fluorophores with TMs under different acidity conditions for summer HULIS.

Zn^{2+} (or Mn^{2+} and Ni^{2+}) and responsive HULIS might be too weak to be observed.

3.4 The hidden mechanism of HULIS with the addition of TMs – taking Cu^{2+} as an example

To further understand the complexation mechanisms of Cu^{2+} and HULIS, the structural variations in HULIS before and after adding 100 µM Cu^{2+} were evaluated by ^{1}H-NMR and FTIR methods, respectively (Figs. 8 and 9). The ^{1}H-NMR results showed that HULIS were rich with protons of H–C, H–C=C–, Ar–H, and H–C–O and functional groups of –OH or –NH, Ar–C=O, Ar–C–O–C, and C–O in both seasons, which were similar to the results of former research (Fan et al., 2013; Hawkins et al., 2016; Kumar et al., 2017). The addition of Cu^{2+} mainly affected the protons bound with aromatics and oxygen in HULIS, with the signals located between δ7 to δ8 and δ3.4 to δ4 ppm trailing off, for which the Ar–H signal decreased by 8.9 % and 2.1 % and the H–C–O signal decreased by 1.4 % and 0.8 % in winter and summer, respectively. According to the basic principles of NMR spectroscopy, coordination or chemical exchange reactions between HULIS molecules and Cu^{2+} might cause the chemical shift signals to vanish or be observed as new signals (Günther, 2013). Meanwhile, the functional groups of HULIS, revealed by FTIR spectra, mainly included –OH (or –NH), –CH, Ph–C=O, C=O, Ph–C–O–C, and –C–O in both seasons, and the summer HULIS contained more oxygen-containing functional groups than winter HULIS because of the high atmospheric oxidization capacity (Chen et al., 2016; Haynes et al., 2019). With the addition of Cu^{2+}, the whole FTIR spectra of winter and summer HULIS blue-shifted to higher energy, especially for O-containing aromatic groups, but the peak shapes remained unchanged, indicating that Cu^{2+} might not directly lead to the transformation of functional groups, but could result in an enhancement of chemical bonds in HULIS molecules.

Our previous research characterized the acidity coefficient, pK_a, and corresponding acidic/basic functional groups of winter and summer HULIS and proposed a hypothetical HULIS structure with unsaturated aromatic main body holding pH-responsive functional groups (Qin et al., 2022). Briefly, values of pK_a of 3.7–3.8 and 8.0–8.1 were assigned as electron-donating groups (represented by H_1A_1 and H_3A_3, respectively), and values of pK_a of 5.0–6.3 were assigned

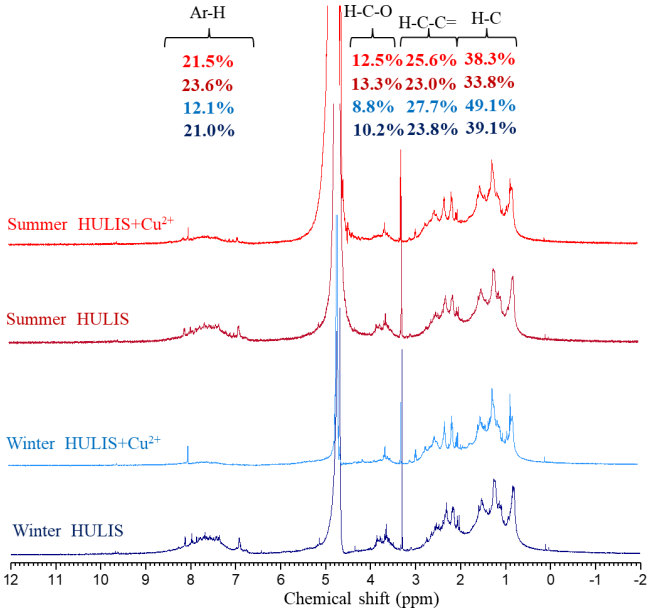

Figure 8. The ^{1}H-NMR spectra of HULIS and HULIS with the addition of 100 µM Cu^{2+} in winter and summer.

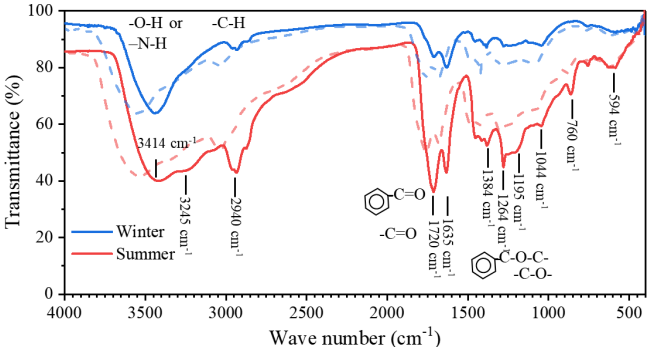

Figure 9. The FTIR spectra of HULIS and HULIS with the addition of 100 µM Cu^{2+} (dash lines) in winter and summer.

as an electron-withdrawing group (represented by H_2A_2) for winter HULIS. Likewise, the pK_a of 6.4 was assigned as an electron-donating group (represented by H_4A_4) and pK_a of 8.4–8.5 was assigned as electron-withdrawing groups (represented by H_5A_5) for summer HULIS. By synthetically considering the versatile optical properties of HULIS with the addition of Cu^{2+} under three acidity conditions and its inherent acid or base groups, the Cu^{2+} and HULIS complexation or interaction mechanisms were explored, and the schematic diagram is depicted in Fig. 10.

1. Firstly, for winter HULIS in the acidic environment, the acidity-sensitive HULIS molecules were hard to deprotonate when H^+ was crowding around. Most of HULIS existed as forms of H_1A_1, H_2A_2, and H_3A_3. Cu^{2+} could easily be absorbed by the electron-donating groups of HULIS to form Cu–A_1H_1 complex or replace the H atom to form Cu–A_1, causing static fluorescence quenching of C1 and C4, which would slightly increase the lifetime of HULIS. Simultaneously, Cu could alter the charge densities of the fluorescent aromatic molecules, leading to an enlargement of conjugated structures and enhancing the fluorescence of C3.

2. Secondly, for winter HULIS in the weakly acidic environment, some of the acidity-sensitive HULIS deprotonated, and the solution contained A_1^-, H_2A_2, and H_3A_3. When added to Cu^{2+}, A_1^- complexed with Cu^{2+} to form Cu–A_1, whereas the sensitive structures of H_2A_2 were electron-donating groups which could hardly provide electrons to Cu^{2+}. However, Cu^{2+} could still be attracted by protons in the unsaturated aromatic structures of HULIS, causing dynamic fluorescence quenching of C2 and C3. With regard to the fast-decreasing lifetime and steady AvgSS of HULIS, chemical reactions might not be involved in these processes and thus flexible structures of Cu–A_2H_2 by electrostatic adsorption or colliding-induced energy transfer could be the possible explanation.

3. Thirdly, for winter HULIS in the neutral environment, the acidity-sensitive HULIS existed as A_1^-, A_2^-, and H_3A_3. The deprotonated HULIS became non-fluorescent, and collision of A_1^- and A_2^- with added Cu^{2+} could not be observed. The fluorescent H_3A_3 could provide electrons to Cu^{2+}, leading to partially fluorescence quenching effects on C1 and C2, and the potential complexation mechanism might be similar to H_1A_1.

4. Lastly, for summer HULIS, the quenching mechanisms of Cu^{2+} and acidity-sensitive HULIS were similar to those of winter HULIS. In the acidic and weakly acidic environment, H_4A_4 and H_5A_5 of summer HULIS were not deprotonated and the quenching effects could have resulted from the replacement of the H atom in H_4A_4 (electron-donating) with Cu^{2+}, causing a decrease in C1–C3. In the neutral environment, Cu^{2+} complexed with deprotonated A_4^- and aromatic structure of H_5A_5 (electron-withdrawing), mainly causing a decrease in C2.

Thus, it was speculated that HULIS with electron-donating groups mainly exhibit fluorescence signals in C1 and C3, which were mainly low-oxidized and highly oxidized humic-like substances, respectively, whereas for HULIS with electron-withdraw groups, the fluorescence signals were mainly exhibited in C2, which was a N-containing species or protein-like species. Besides, although very few studies can clearly explain the interaction mechanisms between HULIS and heavy metals, the hypotheses of the present study are aligned with a recent soil study exploring the retention of heavy metals by humic acid using atomic force microscopy,

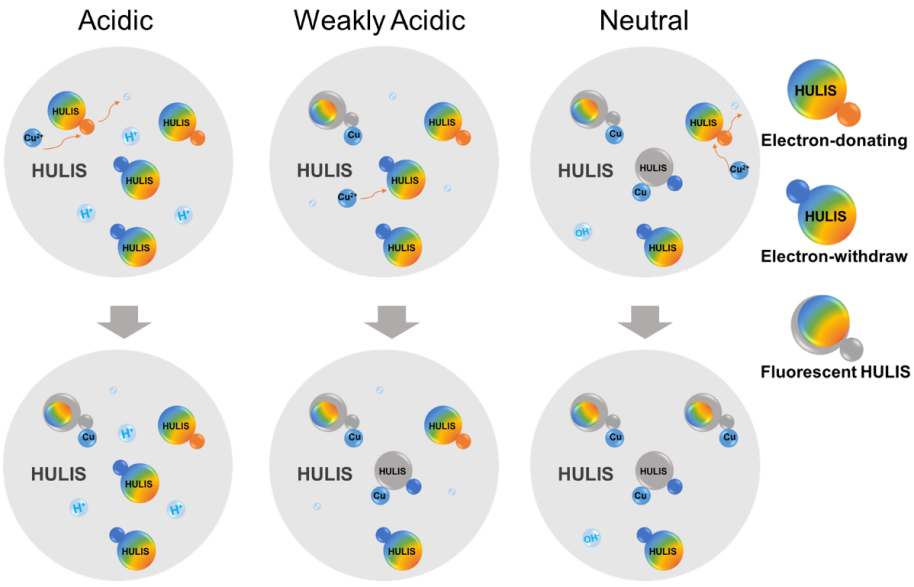

Figure 10. The schematic diagram of HULIS complexation with Cu^{2+} under different acidity conditions.

which found that some metals (Pb^{2+} and Cd^{2+}) formed strong adhesion stems from the synergistic metal-humic acid complexation and cation–π interaction at pH 5.8, leading to significant retention, while other metals (As^{5+} and Cr^{6+}) only bound weakly through hydrogen bonds (Wang et al., 2024).

4 Conclusions and Implications

In this study, the interrelations between the four TMs and HULIS were analyzed by optical methods under acidic, weakly acidic, and near-neutral environments. The results elucidated that the light absorption and fluorescence properties of HULIS were substantially influenced by the solution acidity. TMs either enhance or attenuate the signal strength, contingent on the metal species but with negligible impact on the spectral indices. Cu^{2+} demonstrated the most conspicuous influence on the optical properties of HULIS, while Mn^{2+}, Ni^{2+}, and Zn^{2+} proved to be less responsive. Cu^{2+} could promote light absorption ability of HULIS in a weakly acidic to neutral environment, but the effect was negligible under acidic environment. The ^{1}H-NMR and FTIR spectra of HULIS and HULIS–Cu^{2+} indicated that Cu^{2+} mainly bound with aromatic HULIS, resulting in more compacted molecule structures of HULIS. The distinct tendencies of PARAFAC-separated fluorophores with increasing Cu^{2+} under three acidity conditions indicated that electron-donating groups might correspond to low-oxidized and highly oxidized humic-like substances and Cu^{2+} coupled with HULIS by substituting the H atom, while electron-withdrawing groups were N-containing species or protein-like species, with their fluorescence quenching likely caused by electrostatic adsorption or colliding-induced energy transfer.

Results from this study not only revealed that the complexations of HULIS and TMs could be fragile, but also connected the fluorescence spectra of HULIS with structural characterizations through the micro-effects of TMs on HULIS. HULIS and TMs are both well-known ROS-generative species, and the combined effects of HULIS and TMs on ROS generation can be synergistic or antagonistic depending on the TMs species. The ROS generation abilities of TMs and HULIS that are essentially determined by their physical and chemical properties; interactions, complexation, electrostatic adsorption, and colliding-induced energy transfer processes could enhance or prohibit ROS generation and resulted in a synergistic or antagonistic effect. Our results provide perceptions from a chemical analysis perspective on interactions between HULIS and TMs; however, due to the intricate nature of $PM_{2.5}$, many crucial transition metals, such as Fe^{2+} / Fe^{3+} and Cr^{6+}, which play pivotal roles in the chemical transformation of $PM_{2.5}$ or pose high risks to human health, are not addressed in the current study. Furthermore, comprehensive research on worldwide HULIS samples is also imperative for future investigations.

Data availability. The data used in this study are available on the Zenodo data repository platform at https://doi.org/10.5281/zenodo.10460562 (Qin, 2024).

Supplement. The supplement related to this article is available online at: https://doi.org/10.5194/acp-24-7575-2024-supplement.

Author contributions. TJ and WX designed the experiments, QJ and QY carried them out, SZ and GY helped with the experimental issues, and LJ and SS finished the data analysis. QJ prepared the paper with contributions from all co-authors; ZL, TJ, and WX supervised the writing; and QT provided professional advice on the discussion section.

Competing interests. At least one of the (co-)authors is a member of the editorial board of *Atmospheric Chemistry and Physics*. The peer-review process was guided by an independent editor, and the authors also have no other competing interests to declare.

Disclaimer. Publisher's note: Copernicus Publications remains neutral with regard to jurisdictional claims made in the text, published maps, institutional affiliations, or any other geographical representation in this paper. While Copernicus Publications makes every effort to include appropriate place names, the final responsibility lies with the authors.

Acknowledgements. We would like to thank the editor and anonymous reviewers for their invaluable help in improving the paper.

Financial support. This research has been supported by the National Key Research and Development Program of China (grant nos. 2022YFC3703000, 2023YFE0102400, 2022YFC3703402, and 2022YFC3701103) and the Natural Science Foundation of Hunan Province (grant no. 2023JJ30004).

Review statement. This paper was edited by Joachim Curtius and reviewed by two anonymous referees.

References

Baduel, C., Monge, M. E., Voisin, D., Jaffrezo, J. L., George, C., Haddad, I. E., Marchand, N., and D'Anna, B.: Oxidation of atmospheric humic like substances by ozone: A kinetic and structural analysis approach, Environ. Sci. Technol., 45, 5238–5244, https://doi.org/10.1021/es200587z, 2011.

Chen, Q., Ikemori, F., Higo, H., Asakawa, D., and Mochida, M.: Chemical structural characteristics of hulis and other fractionated organic matter in urban aerosols: Results from mass spectral and FT-IR analysis, Environ. Sci. Technol., 50, 1721–1730, https://doi.org/10.1021/acs.est.5b05277, 2016.

Chen, Q. C., Miyazaki, Y., Kawamura, K., Matsumoto, K., Coburn, S., Volkamer, R., Iwamoto, Y., Kagami, S., Deng, Y. G., Ogawa, S., Ramasamy, S., Kato, S., Ida, A., Kajii, Y., and Mochida, M.: Characterization of chromophoric water-soluble organic matter in urban, forest, and marine aerosols by HR-ToF-AMS analysis and excitation emission matrix spectroscopy, Environ. Sci. Technol., 50, 10351–10360, https://doi.org/10.1021/acs.est.6b01643, 2016.

Chen, W., Habibul, N., Liu, X. Y., Sheng, G. P., and Yu, H. Q.: FT-IR and synchronous fluorescence heterospectral two-dimensional correlation analyses on the binding characteristics of copper onto dissolved organic matter, Environ. Sci. Technol., 49, 2052–2058, https://doi.org/10.1021/es5049495, 2015.

Coble, P., Lead, J., Baker, A., Spencer, R., and Reynolds, D.: Aquatic Organic Matter Fluorescence, Cambridge University Press, https://doi.org/10.1017/CBO9781139045452, 2014.

Fan, X., Song, J., and Peng, P.: Comparative study for separation of atmospheric humic-like substance (HULIS) by ENVI-18, HLB, XAD-8 and DEAE sorbents: elemental composition, FT-IR, ^{1}H-NMR and off-line thermochemolysis with tetramethylammonium hydroxide (TMAH), Chemosphere, 93, 1710–1719, https://doi.org/10.1016/j.chemosphere.2013.05.045, 2013.

Fan, X., Liu, C., Yu, X., Wang, Y., Song, J., Xiao, X., Meng, F., Cai, Y., Ji, W., Xie, Y., and Peng, P.: Insight into binding characteristics of copper (II) with water-soluble organic matter emitted from biomass burning at various pH values using EEM-PARAFAC and two-dimensional correlation spectroscopy analysis, Chemosphere, 278, 130439, https://doi.org/10.1016/j.chemosphere.2021.130439, 2021.

Frka, S., Grgić, I., Turšič, J., Gini, M. I., and Eleftheriadis, K.: Seasonal variability of carbon in humic-like matter of ambient size-segregated water-soluble organic aerosols from urban background environment, Atmos. Environ., 173, 239–247, https://doi.org/10.1016/j.atmosenv.2017.11.013, 2018.

Gali, N. K., Yang, F., Jiang, S. Y., Chan, K. L., Sun, L., Ho, K. F., and Ning, Z.: Spatial and seasonal heterogeneity of atmospheric particles induced reactive oxygen species in urban areas and the role of water-soluble metals, Environ. Pollut., 198, 86–96, https://doi.org/10.1016/j.envpol.2015.01.001, 2015.

Gonzalez, D. H., Cala, C. K., Peng, Q., and Paulson, S. E.: HULIS Enhancement of hydroxyl radical formation from Fe (II): kinetics of fulvic acid-Fe (II) complexes in the presence of lung antioxidants, Environ. Sci. Technol., 51, 7676–7685, https://doi.org/10.1021/acs.est.7b01299, 2017.

Guasco, T. L., Cuadra-Rodriguez, L. A., Pedler, B. E., Ault, A. P., Collins, D. B., Zhao, D., Kim, M. J., Ruppel, M. J., Wilson, S. C., Pomeroy, R. S., Grassian, V. H., Azam, F., Bertram, T. H., and Prather, K. A.: Transition metal associations with primary biological particles in sea spray aerosol generated in a wave channel, Environ. Sci. Technol., 48, 1324–1333, https://doi.org/10.1021/es403203d, 2014.

Günther, H.: NMR Spectroscopy_Basic Principles, Concepts and Applications in Chemistry, ISBN 9783527330003, 2013.

Hawkins, L. N., Lemire, A. N., Galloway, M. M., Corrigan, A. L., Turley, J. J., Espelien, B. M., and De Haan, D. O.: Maillard chemistry in clouds and aqueous aerosol as a source of atmospheric humic-like substances, Environ. Sci. Technol., 50, 7443–7452, https://doi.org/10.1021/acs.est.6b00909, 2016.

Haynes, J. P., Miller, K. E., and Majestic, B. J.: Investigation into photoinduced auto-oxidation of polycyclic aromatic hydrocarbons resulting in brown carbon production, Environ. Sci. Technol., 53, 682–691, https://doi.org/10.1021/acs.est.8b05704, 2019.

Huang, M., Li, Z., Huang, B., Luo, N., Zhang, Q., Zhai, X., and Zeng, G.: Investigating binding characteristics of cadmium and copper to DOM derived from compost and rice straw using EEM-PARAFAC combined with two-dimensional

FTIR correlation analyses, J. Hazard. Mater., 344, 539–548, https://doi.org/10.1016/j.jhazmat.2017.10.022, 2018.

Huang, S. S., Luo, Y., Wang, X., Zhang, T., Lei, Y. L., Zeng, Y. L., Sun, J., Che, H. Z., Xu, H. M., Cao, J. J., and Shen, Z. X.: Optical properties, chemical functional group, and oxidative activity of different polarity levels of water-soluble organic matter in $PM_{2.5}$ from biomass and coal combustion in rural areas in Northwest China, Atmos. Environ., 283, https://doi.org/10.1016/j.atmosenv.2022.119179, 2022.

Kalbitz, K., Geyer, S., and Geyer, W.: A comparative characterization of dissolved organic matter by means of original aqueous samples and isolated humic substances, Chemosphere, 40, 1305–1312, https://doi.org/10.1016/S0045-6535(99)00238-6, 2000.

Kirillova, E. N., Andersson, A., Han, J., Lee, M., and Gustafsson, Ö.: Sources and light absorption of water-soluble organic carbon aerosols in the outflow from northern China, Atmos. Chem. Phys., 14, 1413–1422, https://doi.org/10.5194/acp-14-1413-2014, 2014.

Kumar, V., Goel, A., and Rajput, P.: Compositional and surface characterization of HULIS by UV-Vis, FTIR, NMR and XPS: Wintertime study in Northern India, Atmos. Environ., 164, 468–475, https://doi.org/10.1016/j.atmosenv.2017.06.008, 2017.

Lakowicz, J. R.: Principles of Fluorescence Spectroscopy, Springer US, ISBN 9780387312781, 2006.

Li, J., Chen, Q., Sha, T., and Liu, Y.: Significant promotion of light absorption ability and formation of triplet organics and reactive oxygen species in atmospheric HULIS by Fe (III) ions, Environ. Sci. Technol., 56, 16652–16664, https://doi.org/10.1021/acs.est.2c05137, 2022.

Lin, M. and Yu, J. Z.: Effect of metal-organic interactions on the oxidative potential of mixtures of atmospheric humic-like substances and copper/manganese as investigated by the dithiothreitol assay, Sci. Total. Environ., 697, 134012, https://doi.org/10.1016/j.scitotenv.2019.134012, 2019.

Lin, P., Engling, G., and Yu, J. Z.: Humic-like substances in fresh emissions of rice straw burning and in ambient aerosols in the Pearl River Delta Region, China, Atmos. Chem. Phys., 10, 6487–6500, https://doi.org/10.5194/acp-10-6487-2010, 2010.

Ma, L., Li, Z., Yabo, S. D., Li, B., Sun, S., and Qi, H.: Insight into the interaction between heavy metals and water-soluble organic compounds in $PM_{2.5}$ affected by heavy haze using ultraviolet–visible and fluorescence spectra combined with two-dimensional correlation spectroscopy, J. Clean Prod., 362, 132476, https://doi.org/10.1016/j.jclepro.2022.132476, 2022.

Ma, Y., Cheng, Y., Qiu, X., Cao, G., Kuang, B., Yu, J. Z., and Hu, D.: Optical properties, source apportionment and redox activity of humic-like substances (HULIS) in airborne fine particulates in Hong Kong, Environ. Pollut., 255, 113087, https://doi.org/10.1016/j.envpol.2019.113087, 2019.

Mao, J., Fan, S., Jacob, D. J., and Travis, K. R.: Radical loss in the atmosphere from Cu-Fe redox coupling in aerosols, Atmos. Chem. Phys., 13, 509–519, https://doi.org/10.5194/acp-13-509-2013, 2013.

Mo, Y., Li, J., Cheng, Z., Zhong, G., Zhu, S., Tian, C., Chen, Y., and Zhang, G.: Dual carbon isotope-based source apportionment and light absorption properties of water-soluble organic carbon in $PM_{2.5}$ over China, J. Geophy. Res.-Atmos., 126, e2020JD033920, https://doi.org/10.1029/2020jd033920, 2021.

Paris, R. and Desboeufs, K. V.: Effect of atmospheric organic complexation on iron-bearing dust solubility, Atmos. Chem. Phys., 13, 4895–4905, https://doi.org/10.5194/acp-13-4895-2013, 2013.

Park, S. S. and Yu, J.: Chemical and light absorption properties of humic-like substances from biomass burning emissions under controlled combustion experiments, Atmos. Environ., 136, 114–122, https://doi.org/10.1016/j.atmosenv.2016.04.022, 2016.

Parlanti, E., Worz, K., Geoffroy, L., and Lamotte, M.: Dissolved organic matter fluorescence spectroscopy as a tool to estimate biological activity in a coastal zone submitted to anthropogenic inputs, Org. Geochem., 31, 1765–1781, https://doi.org/10.1016/s0146-6380(00)00124-8, 2000.

Qin, J.: Data for manuscript Measurement Report: Effects of transition metal ions on the optical properties of humic-like substances revealing structural preference, Zenodo [data set], https://doi.org/10.5281/zenodo.10460562, 2024.

Qin, J., Zhang, L., Zhou, X., Duan, J., Mu, S., Xiao, K., Hu, J., and Tan, J.: Fluorescence fingerprinting properties for exploring water-soluble organic compounds in $PM_{2.5}$ in an industrial city of northwest China, Atmos. Environ., 184, 203–211, https://doi.org/10.1016/j.atmosenv.2018.04.049, 2018.

Qin, J., Zhang, L., Qin, Y., Shi, S., Li, J., Gao, Y., Tan, J., and Wang, X.: pH-Dependent chemical transformations of humic-like substances and further cognitions revealed by optical methods, Environ. Sci. Technol., 56, 7578–7587, https://doi.org/10.1021/acs.est.1c07729, 2022.

Ryan, D., Thompson, C. P., and Weber, J. H.: Comparison of Mn^{2+}, Co^{2+}, and Cu^{2+} binding to fulvic acid as measured by fluorescence quenching, Can. J. Chem., 61, 1505–1509, https://doi.org/10.1139/v83-262, 1983.

Saleh, R., Robinson, E. S., Tkacik, D. S., Ahern, A. T., Liu, S., Aiken, A. C., Sullivan, R. C., Presto, A. A., Dubey, M. K., Yokelson, R. J., Donahue, N. M., and Robinson, A. L.: Brownness of organics in aerosols from biomass burning linked to their black carbon content, Nat. Geosci., 7, 647–650, https://doi.org/10.1038/ngeo2220, 2014.

Scheinhardt, S., Müller, K., Spindler, G., and Herrmann, H.: Complexation of trace metals in size-segregated aerosol particles at nine sites in Germany, Atmos. Environ., 74, 102–109, https://doi.org/10.1016/j.atmosenv.2013.03.023, 2013.

Slikboer, S., Grandy, L., Blair, L. S., Nizkorodov, A. S., Smith, W. R., and Al-Abadleh, A. H.: Formation of Light Absorbing Soluble Secondary Organics and Insoluble Polymeric Particles from the Dark Reaction of Catechol and Guaiacol with Fe(III), Environ. Sci. Technol., 49, 7793–7801, https://doi.org/10.1021/acs.est.5b01032, 2015.

Strickler, S. J. and Berg, R. A.: Relationship between absorption intensity and fluorescence lifetime of molecules, J. Chem. Phys., 37, 814–822, https://doi.org/10.1063/1.1733166, 1962.

Verma, V., Rico-Martinez, R., Kotra, N., King, L., Liu, J., Snell, T. W., and Weber, R. J.: Contribution of water-soluble and insoluble components and their hydrophobic/hydrophilic subfractions to the reactive oxygen species-generating potential of fine ambient aerosols, Environ. Sci. Technol., 46, 11384–11392, https://doi.org/10.1021/es302484r, 2012.

Wang, H., Zhang, L., Huo, T., Wang, B., Yang, F., Chen, Y., Tian, M., Qiao, B., and Peng, C.: Application of parallel factor analysis model to decompose excitation-emission ma-

trix fluorescence spectra for characterizing sources of water-soluble brown carbon in $PM_{2.5}$, Atmos. Environ., 223, 117192, https://doi.org/10.1016/j.atmosenv.2019.117192, 2020.

Wang, X., Qin, Y., Qin, J., Long, X., Qi, T., Chen, R., Xiao, K., and Tan, J.: Spectroscopic insight into the pH-dependent interactions between atmospheric heavy metals (Cu and Zn) and water-soluble organic compounds in $PM_{2.5}$, Sci. Total. Environ., 767, 145261, https://doi.org/10.1016/j.scitotenv.2021.145261, 2021.

Wang, Z., Lu, Q., Liu, C., Tian, H., Wang, J., Xie, L., Liu, Q., and Zeng, H.: Nanoscale insights into the interaction mechanism underlying the adsorption and retention of heavy metal ions by humic acid, Environ. Sci. Technol., 58, 3412–3422, https://doi.org/10.1021/acs.est.3c08309, 2024.

Win, M. S., Tian, Z., Zhao, H., Xiao, K., Peng, J., Shang, Y., Wu, M., Xiu, G., Lu, S., Yonemochi, S., and Wang, Q.: Atmospheric HULIS and its ability to mediate the reactive oxygen species (ROS): A review, J. Environ. Sci.-China, 71, 13–31, https://doi.org/10.1016/j.jes.2017.12.004, 2018.

Wu, C., Yang, J., Fu, Q., Zhu, B., Ruan, T., and Jiang, G.: Molecular characterization of water-soluble organic compounds in $PM_{2.5}$ using ultrahigh resolution mass spectrometry, Sci. Total. Environ., 668, 917–924, https://doi.org/10.1016/j.scitotenv.2019.03.031, 2019.

Xiao, K., Liang, S., Xiao, A., Lei, T., Tan, J., Wang, X., and Huang, X.: Fluorescence quotient of excitation-emission matrices as a potential indicator of organic matter behavior in membrane bioreactors, Environ. Sci.-Wat. Res., 4, 281–290, https://doi.org/10.1039/C7EW00270J, 2018.

Xiao, K., Han, B., Sun, J., Tan, J., Yu, J., Liang, S., Shen, Y., and Huang, X.: Stokes shift and specific fluorescence as potential indicators of organic matter hydrophobicity and molecular weight in membrane bioreactors, Environ. Sci. Technol., 53, 8985–8993, https://doi.org/10.1021/acs.est.9b02114, 2019.

Xiao, K., Yu, J., Wang, S., Du, J., Tan, J., Xue, K., Wang, Y., and Huang, X.: Relationship between fluorescence excitation-emission matrix properties and the relative degree of DOM hydrophobicity in wastewater treatment effluents, Chemosphere, 254, 126830, https://doi.org/10.1016/j.chemosphere.2020.126830, 2020.

Yamashita, Y. and Jaffe, R.: Characterizing the interactions between trace metals and dissolved organic matter using excitation-emission matrix and parallel factor analysis, Environ. Sci. Technol., 42, 7374–7379, https://doi.org/10.1021/es801357h, 2008.

Yang, W., Zhang, T., Han, C., Tang, N., Yang, H., and Xue, X.: Photoenhanced heterogeneous reaction of O_3 with humic acid: Focus on O_3 uptake and changes in the composition and optical property, Environ. Pollut., 268, 115696, https://doi.org/10.1016/j.envpol.2020.115696, 2021.

Ye, C., Chen, H., Hoffmann, E. H., Mettke, P., Tilgner, A., He, L., Mutzel, A., Bruggemann, M., Poulain, L., Schaefer, T., Heinold, B., Ma, Z., Liu, P., Xue, C., Zhao, X., Zhang, C., Zhang, F., Sun, H., Li, Q., Wang, L., Yang, X., Wang, J., Liu, C., Xing, C., Mu, Y., Chen, J., and Herrmann, H.: Particle-phase photoreactions of HULIS and TMIs establish a strong source of H_2O_2 and particulate sulfate in the winter North China Plain, Environ. Sci. Technol., 55, 7818–7830, https://doi.org/10.1021/acs.est.1c00561, 2021.

Yu, J., Xiao, K., Xue, W., Shen, Y.-x., Tan, J., Liang, S., Wang, Y., and Huang, X.: Excitation-emission matrix (EEM) fluorescence spectroscopy for characterization of organic matter in membrane bioreactors: Principles, methods and applications, Front. Env. Sci. Eng., 14, 31, https://doi.org/10.1007/s11783-019-1210-8, 2020.

Zanca, N., Lambe, A. T., Massoli, P., Paglione, M., Croasdale, D. R., Parmar, Y., Tagliavini, E., Gilardoni, S., and Decesari, S.: Characterizing source fingerprints and ageing processes in laboratory-generated secondary organic aerosols using proton-nuclear magnetic resonance (1H-NMR) analysis and HPLC HULIS determination, Atmos. Chem. Phys., 17, 10405–10421, https://doi.org/10.5194/acp-17-10405-2017, 2017.

Zhang, T., Shen, Z., Huang, S., Lei, Y., Zeng, Y., Sun, J., Zhang, Q., Ho, S. S. H., Xu, H., and Cao, J.: Optical properties, molecular characterizations, and oxidative potentials of different polarity levels of water-soluble organic matters in winter $PM_{2.5}$ in six China's megacities, Sci. Total. Environ., 853, 158600, https://doi.org/10.1016/j.scitotenv.2022.158600, 2022.

Zhu, Y., Jin, Y., Liu, X., Miao, T., Guan, Q., Yang, R., and Qu, J.: Insight into interactions of heavy metals with livestock manure compost-derived dissolved organic matter using EEM-PARAFAC and 2D-FTIR-COS analyses, J. Hazard. Mater., 420, 126532, https://doi.org/10.1016/j.jhazmat.2021.126532, 2021.